Electrically Tunable Topological State in [111] Perovskite Materials with Antiferromagnetic Exchange Field

Qi-Feng Liang,[1,2] Long-Hua Wu,[1] and Xiao Hu[1]

[1]*International Center for Materials Nanoarchitectornics (WPI-MANA) National Institute for Materials Science, Tsukuba 305-0044, Japan*

[2]*Department of Physics, Shaoxing University, Shaoxing 312000, China*

(Dated: January 18, 2013)

A topological state with simultaneous nonzero Chern number and spin Chern number is possible for electrons on honeycomb lattice based on band engineering by staggered electric potential and antiferromagnetic exchange field in presence of intrinsic spin-orbit coupling. With first principles calculation we confirm that the scheme can be realized by material modification in perovskite G-type antiferromagnetic insulators grown along [111] direction, where d electrons hop on a single buckled honeycomb lattice. This material is ideal for spintronics applications, since it provides a spin-polarized quantized edge current, robust to both nonmagnetic and magnetic defects, with the spin polarization tunable by inverting electric field.

PACS numbers: 73.20.-r, 73.43.-f, 03.65.Vf, 75.70.Tj

Introduction.—The discovery of quantum Hall effect (QHE) by von Klitzing opened a new chapter in condensed matter physics. It was revealed [1, 2] that the integer coefficient in Hall conductance is nothing but the Chern number labeling the topological property of the electron wavefunction. Since then to explore possible topological states has been one of the main driving forces in study of condensed matter physics[3–10].

The breakthrough took place when Kane and Mele clarified that electrons on graphene, a two-dimensional honeycomb lattice of carbon atoms, open a gap by spin-orbit coupling (SOC) and achieve a topologically nontrivial state called quantum spin Hall effect (QSHE) [4]. It turned out that in graphene the intrinsic SOC is very small which makes detection of QSHE hopeless. QSHE was then predicted theoretically [5] and realized experimentally in HgTe quantum well with strong SOC [6].

As the common homebase for both Kane-Mele model [4]and the spinless Haldane model [3], honeycomb lattice serves a unique role in understanding the topological property of electron systems. It may be illustrative to summarize its electronic structure paying attention to the Berry curvature configuration [11]. There are two sites in the unit cell of honeycomb structure. With nearest neighbor hopping, electronic valance and conduction bands touch linearly and thus form Dirac cones at two inequivalent k points, K and K′, locating at the corners of Brillouin zone. It is important to observe that Bloch wavefunctions exhibit opposite chiral features around K and K′, characterized by opposite Berry curvatures, which establishes the special position of honeycomb lattice in exploring topological state.

With time-reversal symmetry, the Berry curvatures in spin-up and spin-down channels overlap as shown in figure 1(a). Introducing intrinsic SOC opens a gap at the two Dirac cones, and flips Berry curvatures at K in spin-up channel and at K′ in spin-down channel preserving time-reversal symmetry, which results in the Berry curvature configuration in figure 1(b), characterizing the QSHE state [4]. One can further flip the Berry curvatures at K in both spin-up and spin-down channels, yielding the configuration figure 1(c) (a topologically trivial state), by a field conjugate to the valley degree of freedom such as the polarized field [12–15]. With an additional staggered electric field, which can be realized in silicene with buckled honeycomb lattice in terms of a uniform electric field[16], Ezawa could flip the Berry curvature at K in only one spin channel, resulting in figure 1(e) characterized by simultaneous nonzero charge Chern number and spin Chern number [15] (see also [17–19]). The band engineering is based on a full control on the degrees of freedom of spin, valley and sublattice, taking advantages of the intrinsic SOC. By the way, the Berry curvature configuration in figure 1(d) corresponds to quantum anomalous Hall effect (QAHE)[18–23].

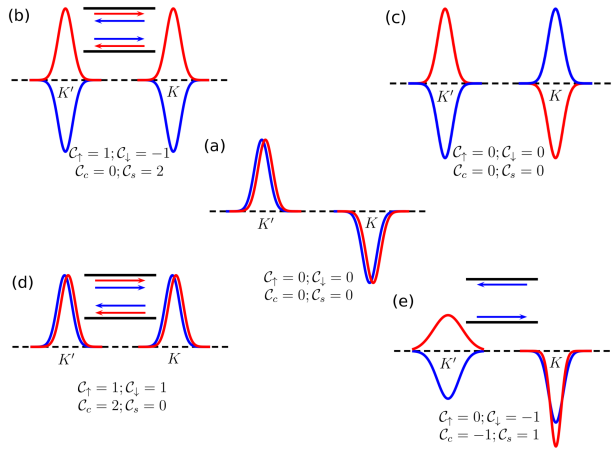

FIG. 1: (Colour online) Schematics for possible configurations of Berry curvatures and Chern numbers for insulating states on honeycomb lattice: (a) pristine honeycomb lattice, (b) QSHE, (c) trivial state with broken time-reversal symmetry, (d) QAHE, (e) topological state with simultaneous nonzero charge and spin Chern numbers.

In the present paper we notice that in presence of intrinsic SOC, a staggered magnetic field plays a similar role as provided by the polarized light proposed by Ezawa[15]. Since the staggered magnetic field can be realized by antiferromagnetic (AFM) insulators, compact and stable devices based on the topological state in figure 1(e) are possible as compared with the photo-assisted scheme.

As material realization of our idea, we focus on d-electron systems in perovskite structure[24]. First, we choose a perovskite insulator ABO_3 with G-type AFM order on the magnetic B atoms. As first discussed by Xiao et al.[9], along [111] direction B atoms form a stacking of buckled honeycomb lattice, which can be grown by cutting-edge molecular beam epitaxy (MBE) with atomic precision [25]. During the growing process, a single buckled honeycomb layer of B atoms is replaced by that of nonmagnetic B′ atoms, where the element B′ is chosen conjugate to B in order to form a d^8 configuration. For B′-d electrons on the single buckled honeycomb lattice, intrinsic SOC becomes sizable, a uniform electric field induces a staggered electric potential for the two sublattices, and the G-type AFM order on B atoms on the two sides provides an AFM exchange field. The material design makes the magnetic field of pure exchange character, which avoids possible stray field from permanent ferromagnet. We have checked successfully our idea by performing first principles calculations for several materials. In transition metal perovskites we found intrinsic SOC of several tens of meV, which is larger than that in silicene in magnitude by one order, and makes the new topological state available at room temperature.

Effective model and phase diagram.— Let us illustrate our scheme based on the four-band Hamiltonian for electrons on a buckled honeycomb lattice under an AFM exchange field and a uniform electric field perpendicular to the plane [26]

$$H = \sigma_x k_x + \tau_z \sigma_y k_y + \lambda \sigma_z \tau_z s_z + V\sigma_z + M\sigma_z s_z, \quad (1)$$

around the two inequivalent K and K′ points where the z axis is taken along the [111] direction of peroskite structure; σ's are Pauli matrices for sublattice, and $\tau_z = \pm 1$ and $s_z = \pm 1$ are binary degrees of freedom referring to valley and spin. The first two terms come from the nearest neighbor hopping same as that in a pristine graphene [26]; the third term is for the intrinsic SOC with a positive coupling coefficient $\lambda > 0$ by definition, which can be large due to the heavier host transition metal atom and the buckled structure; the fourth term is induced by a uniform electric potential on the buckled structure, and the last term is the AFM exchange field. The chemical potential is set to zero, and all energies are measured in units of the nearest neighbor hopping integral in the present work. As will be shown later, this model Hamiltonian describes the low-energy physics of transition metal oxides with perovskite structure grown along [111] direction.

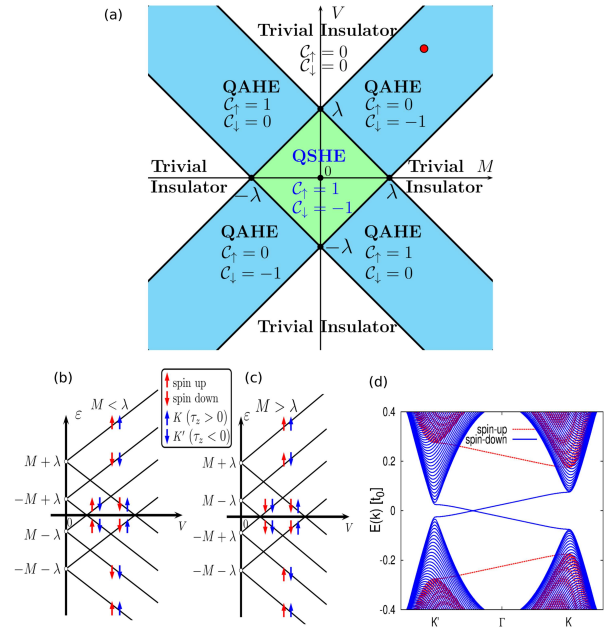

FIG. 2: (Colour online) (a) Phase diagram for staggered electric potential V and antiferromagnetic field M, with presumed positive intrinsic SOC $\lambda > 0$; (b) and (c) schematic diagram for energy level crossing upon electric field tuning for $M < \lambda$ and $M > \lambda$; (d) band structure for $N = 100$ zigzag ribbon of honeycomb lattice with $V = 0.25$, $M = 0.2$ and $\lambda = 0.1$ (red dot in (a)).

tion.

We reveal behaviors of the system below upon tuning the electric potential V while the M field and λ are fixed, corresponding directly with our material design and experimental manipulation. For $0 < M < \lambda$, the gaps are topologically nontrivial for both spin-up and spin-down channels for $V = 0$, characterizing the QSHE state (see figure 1(c)). As illustrated in figure 2(b), when V increases, the gap for spin-up channel shrinks, closes and reopens at K′ point (τ_z=-1) for $V = \lambda - M$. This quantum phase transition turns the spin-up channel to a trivial state, while the spin-down channel remains nontrivial. This insulating state exhibiting nontrivial gap in only one spin channel is different from other topological states such as QSHE and QAHE, as discussed by Ezawa [15]. When V increases further, the gap for spin-down channel shrinks, closes and reopens at K point (τ_z=1) for $V = \lambda + M$, which makes the spin-down channel trivial as well, and the system transforms to a trivial insulating state via a second quantum phase transition.

For $M > \lambda$, the system exhibits trivial gaps in both spin-up and -down channels for $V = 0$ (see figure 1(c)). As seen in figure 2(c), when V increases, the gap for spin-down channel shrinks, closes and reopens at $\tau_z = -1$ for $V = M - \lambda$, which brings the spin-down channel into a topological state. When V increases further, the gap in spin-down channel shrinks, closes and reopens at $\tau_z = 1$ for $V = \lambda + M$, which drives the system back to a trivial

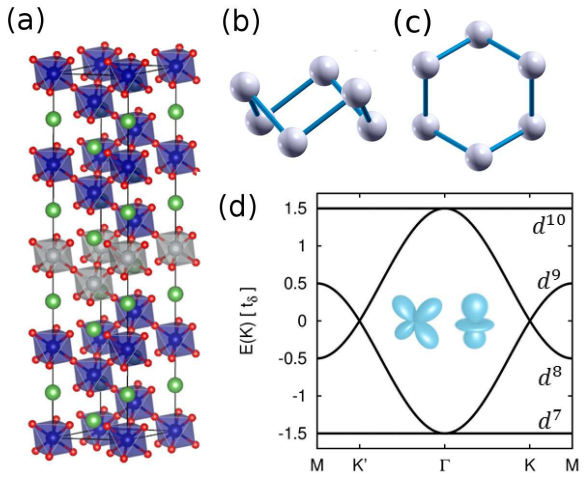

FIG. 3: (Colour online) (a) A 6-Layer ABB′X perovskite with one layer of B (blue) replaced by B′ (grey). (b) and (c) Side and top views of the buckled honeycomb lattice formed by B′ cations. (d) Noninteracting tight-binding band structure of the e_g system, where each band is labeled with the corresponding electron configuration if it is occupied. Inset shows the two e_g orbits of B′.

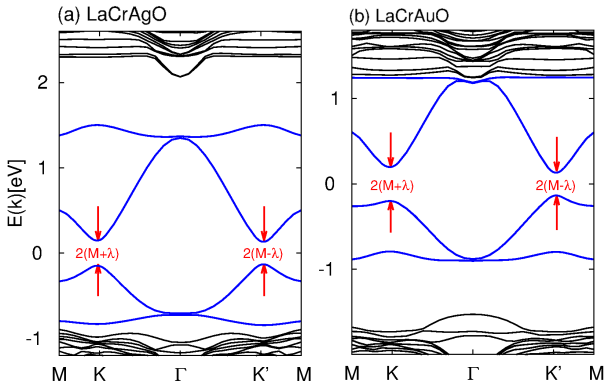

FIG. 4: (Colour online) Band structures based on first-principles calculation on LaCrAgO and LaCrAuO with a super unit cell $(A_2B'_2O_6)/(A_2B_2O_6)_5$ along the [111] direction.

TABLE I: Parameters for AFM order and SOC fit from GGA+U+SOC calculation. For KNiInF and KNiTlF the electronic configurations of In^{2+} and Tl^{2+} are $5s^1$ and $6s^1$.

field [meV]	LaCrAgO	LaCrAuO	LaFeAgO	LaFeAuO
M	141	166	541	467
λ	7.30	32.91	7.31	33.52
KNiPdF	KNiPtF	KNiInF*	KNiTlF*	
625	504	290	235	
11.38	33.40	5.05	18.58	

insulator state.

Based on the above analysis we can compose the full phase diagram as displayed in figure 2(a) by symmetry consideration. The new topological state is realized when the absolute values of the three fields $|V|$ and $|M|$ and $|\lambda|$ form a triangle, which indicates clearly that the intervening among the three degrees of freedom, σ_z, τ_z and s_z is crucial for the new topological state. A typical band structure for zigzag ribbon of the buckled honeycomb lattice is displayed in figure 2(d); there are two edge states crossing fermi level which are localized at the opposite edges (see figure 1(e)). The present phase diagam is similar to the one by Ezawa [15], except for that the states with same Chern numbers lie in diagonal directions in the present one, while locating in same half spaces in that by Ezawa [15], due to the difference of controlling fields in the two Hamiltonians.

Material realization.— In perovskite ABO_3 material shown in figure 3(a), A and B form two penetrating simple cubic lattices. The octahedron cage formed by six oxygens around the transition metal B generates the doublet e_g and triplet t_{2g} orbits of the d electrons. In the [111] direction, a simple cubic structure can be viewed as a stacking of buckled honeycomb lattices as shown in figures 3(b) and (c). In the new coordinate, intrinsic SOC appears between the two e_g orbits. In regard of material synthesis, recent developments in laser molecular beam epitaxy (MBE) technique permit one to grow perovskite structure along [111] direction with atomic precision [25]. All these make the d electrons in perovskite structure a very hopeful platform for realizing topological states, as illustrated first by Xiao et al. [9].

Many transition metal oxides with perovskite structure are known as wide-gap antiferromagnetic insulator. A subgroup of these materials presume the so-called G-type AMF order where spins align antiferromagnetically in the two sublattices of the buckled honeycomb lattice. This is the playground where we perform material design and field manipulation to realize topological state with our scheme. We replace one buckled layer of B by a nonmagnetic element B′, and obtain B′-d electrons on a single layer of buckled honeycomb lattice, which feel AFM exchange field from the G-type AMF order of the host material ABO_3 [27].

There is a gap (10Dq) between the e_g and t_{2g} orbits, which drops t_{2g} orbits from the low-energy physics. In each unit cell, two B′ atoms contribute totally four e_g orbits. The band structure for these four orbits is shown in figure 3(d) based on a tight-binding Hamiltonian with the hopping integrals given by Slater-Koster formula. One finds two flat bands and two dispersive bands crossing each other. Xiao et al. [9, 18, 19] focus on the flat band and developed an interesting scenario for possible topological state based on strong electron correlations by using $d^7(t_{2g}^6 e_g^1)$ configuration. Here we concentrate on the two dispersive bands by taking $d^8(t_{2g}^6 e_g^2)$ systems for which the fermi level is around their crossing point.

In order to verify the above picture, we have performed first principles calculation on the host material $LaCrO_3$ with one layer of $La_2Ag_2O_6$ or $La_2Au_2O_6$ inserted, which

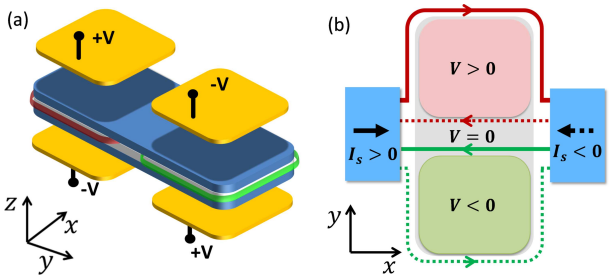

FIG. 5: (Colour online) Device for a "composite QHSE" insulator formed by two copies of the new topological state.

realizes a $d^8(t_{2g}^6 e_g^2)$ system on the buckled honeycomb lattice. The super cell used in the calculations contains 6 layers with a configuration of $(La_2B'_2O_6)/(La_2B_2O_6)_5$. The calculations are performed by using density functional theory(DFT) within the generalized gradient approximation (GGA) approach in the parametrization of Perdew, Burke and Ehzorhof (PBE) [28] for exchage-correlation as implemented in the Vienna Ab Initio Simulation Package (VASP) [29]. The bulk lattice constant is set to $3.85\mathring{A}$ for $LaCrO_3$ and atoms are allowed to relax inside the super cell. The on-site Coulomb interactions of the $3d$ electrons of Cr are treated by Dudarev' method with an effective U value [30], U_{eff}=U-J=5.4eV. We have checked that our main results are valid for a large window of the U values. The momentum space-mesh is $6 \times 6 \times 1$ and the cutoff energy is 440eV.

The band structures of LaCrAgO and LaCrAuO obtained from GGA+U+SOC calculations are displayed in figures 4(a) and (b). First of all, the two flat bands and two dispersive bands close to the fermi level in figure 3(d) are realized in the two materials. The two gaps at K and K′, which were absent in figure 3(b) for tight-binding model, are induced by the AFM exchange field from $LaCrO_3$ and the SOC. From the two gaps at K and K′, we figure out $M = 0.141$eV and $\lambda = 7.3$meV for LaCrAgO, and $M = 0.166$eV and $\lambda = 32.91$meV for LaCrAuO. We have also calculated several other possible materials and the results are summarized in TABLE 1. As the maximal nontrivial gap is given by 2λ, the results from first principles calculations suggest that a topological material may be realized at room temperature. Typical electric field to realize the new topological state in the order of $0.1\text{V}/\mathring{A}$.

Possible applications.— This new topological state available probably at room temperature is ideal for spintronics applications, since it provides a spin-polarized quantized edge current, robust to both nonmagnetic and magnetic defects, with the spin polarization tunable by inverting electric field.

Using two copies of the new topological state, one can realize a "composite QSHE insulator". As shown in figure 5(a), we fabricate two pairs of electrodes (golden) with opposite bias voltages. The two patches exhibit states with opposite chiralities and spins. Spin Hall conductance can be measured based on this device. As shown in figure 5(b), when a positive spin current I_s is injected from the left electrode, the out-going spin-up current flows from the left electrode along the top edge of upper patch (upturned red solid curve), while the in-going spin-down current flows into the left electrode along the straight line between the two electrodes (solid green line), which results in zero charge current. Because charge current flows only on the top edge and cumulates charges there, a Hall voltage drop can be detected between the top and bottom edges of the device. As compared with the QSHE realized before, even a time-reversal-symmetry-broken perturbation, e.g., a magnetic field or magnetic impurities cannot backscatter the counter charge currents with spin up and down at the center of the device, since the charge currents are now distributed in different patches as shown in figure 5(b).

Discussions.— The present topological state is robust against Rashba SOC [22, 23], which, although small, should be present since the electric field breaks the inversion symmetry with respect to the honeycomb lattice plane. Actually, it is known that in graphene the nontrivial band gap closes for $\lambda_R > \lambda$ and the QSHE will be destroyed[4] due to the mixing of the two spin channels by Rashba SOC. In the new topological state with for example $V = M > 0$, a gap of $2(2M - \lambda)$ is opened in spin-up channel whereas the gap in the spin-down channel is 2λ. Since $M \gg \lambda$ as shown in Table 1, even a Rashba SOC stronger than the intrinsic one $\lambda_R \gtrsim \lambda$ cannot close the gap by mixing the two spin channels.

Note.— About finishing our manuscript, we became aware of a recent work by Ezawa arXiv.1301.0971, addressing the same physics. In his work, the staggered magnetic field is generated by two ferromagnets on the two sides of silicene layer.

Acknowledgements.— X.H. is grateful to Masashi Tachiki and Seiji Miyashita for helpful discussions. This work was supported by WPI Initiative on Materials Nanoarchitectonics, MEXT of Japan, and Grants-in-Aid for Scientific Research (No.22540377), JSPS, and partially by CREST, JST. Q.F.L. is also supported by NSFC under grants 10904092.

[1] Thouless D J, Kohmoto M, Nightingale M P and den Nijs M 1982 *Phys. Rev. Lett.* **49** 405

[2] Niu Q, Thouless D J and Wu Y S 1985 *Phys. Rev. B* **31** 3372

[3] Haldane F D M 1988 *Phys. Rev. Lett.* **61** 2015
[4] Kane C L and Mele E J 2005 *Phys. Rev. Lett.* **95** 226801
[5] Bernevig B A, Hughes T L and Zhang S C 2006 *Science* **314** 1757
[6] König M, Wiedmann S, Brüne C, Roth A, Buhmann H, Molenkamp L W, Qi X L and Zhang S C 2007 *Science* **318** 766
[7] Hasan M and Kane C L 2010 *Rev. Mod. Phys.* **82** 3045
[8] Qi X L and Zhang S C 2011 *Rev. Mod. Phys.* **83** 1057
[9] Xiao D, Zhu W, Ran Y, Nagaosa N and Okamato S 2011 *Nature Comm.* **2** 596
[10] Yang Y, Xu Z, Sheng L, Wang B G, Xing D Y and Sheng D N 2011 *Phys. Rev. Lett.* **107** 066602
[11] Xiao D, Shi J and Niu Q 2005 *Phys. Rev. Let.* **95** 137204; Thonhauser T, Ceresoli D, Vanderbilt D and Resta R 2005 *ibid* **95** 137205
[12] Xiao D, Yao W and Niu Q 2007 *Phys. Rev. Lett.* **99** 236809
[13] Zeng H, Dai J, Yao W, Xiao D and Cui X 2012 *Nature Nanotech.* **7** 490
[14] Mak K F, He K, Shan J and Heinz T F 2012 *Nature Nanotech.* **7** 494
[15] Ezawa M 2013 *Phys. Rev. Lett.* **110** 026603
[16] Ni Z, Liu Q, Tang K, Zheng J, Zhou J, Qin R, Gao Z, Yu D and Lu J 2011 *Nano Lett.* **12** 113
[17] Liu C X, Qi X L, Dai X, Fang Z and Zhang S C 2008 *Phys. Rev. Lett.* **101** 146802
[18] Rüegg A, Fiete G A 2011 *Phys. Rev. B* **84** 201103(R)
[19] Yang K Y, Zhu W, Xiao D, Okamoto S, Wang Z and Ran Y 2011 *Phys. Rev. B* **84** 201104(R)
[20] Nagaosa N, Sinova J, Onoda S, MacDonald A H and Ong N P 2010 *Rev. Mod. Phys.* **82** 1539
[21] Yu R, Zhang W, Zhang H J, Zhang S C, Dai X and Fang Z 2010 *Science* **329** 61
[22] Qiao Z, Yang S A, Feng W, Tse W K, Ding J, Yao Y, Wang J and Niu Q 2010 *Phys. Rev. B* **82** 161414(R)
[23] Ezawa M 2012 *Phys. Rev. Lett.* **109** 055502
[24] Mitchell R H, Perovskites 2002 *Perovskites: Modern and Ancient* (Almaz Press Inc., Ontario Canada)
[25] Ueda K, Tabata H and Kawai T 1998 *Science* **280** 1064
[26] For d^8 system where the electronic structures involves two degenerated e_g orbits, one can still obtain an effective H_0 by reducing a 4-band hamiltonian into a 2-band one using $k \cdot p$ perturbation theory.
[27] Actually there are two magnetic configurations which have similar energies. From our first principle calculation, we found the one which induces the desired AFM magnetizaiton in the AB'O3 layer always has a lower energy.
[28] Perdew J P, Burke K and Ernzerhof M 1996 *Phys. Rev. Lett.* **77** 3865
[29] Kresse G and Furthmüller J 1996 *Phys. Rev. B* **54** 11169
[30] Dudarev S L, Botton G A, Savrasov S Y, Humphreys C J, Sutton A P 1998 *Phys. Rev. B* **57** 1505